

## Electric Supplementary Information

### **Li<sup>+</sup> conducting garnet-type oxides sintering triggered by H<sup>+</sup>/Li<sup>+</sup> ion-exchange reaction**

Shingo Ohta\*, Masatsugu Kawakami, Hiroshi Nozaki, Chihiro Yada, Toshiya Saito and Hideki Iba

Advanced Material Engineering Division, Higashifuji Technical Center, Toyota Motor Corporation, 1200 Mishuku, Susono, Shizuoka 410-1193, Japan

E-mail: [sohta@mosk.tytlabs.co.jp](mailto:sohta@mosk.tytlabs.co.jp)

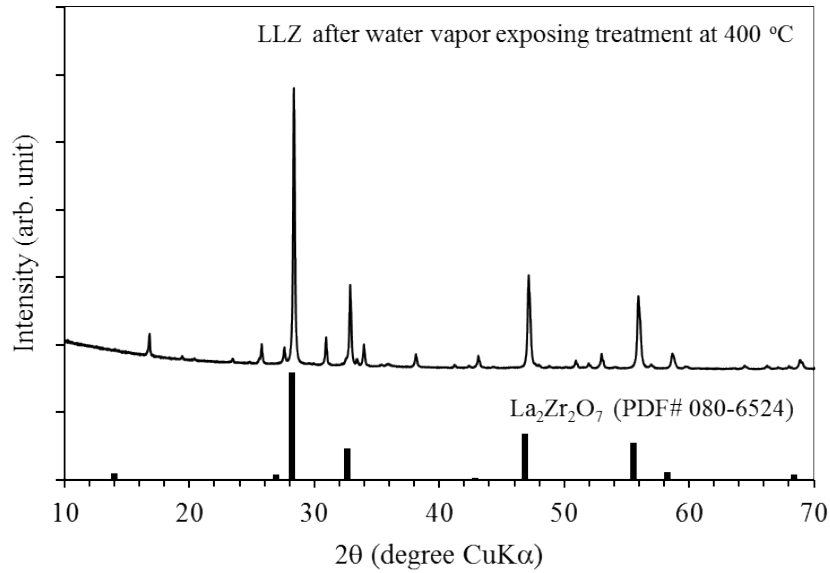


**Figure S1** XRD pattern of LLZ after water vapor exposure treatment at 400 °C

The pellet molded body of LLZ particles was exposed to water vapor at 400 °C for 12 h. Crystal structure transformation to the pyrochlore structure and other unknown phases was confirmed, which suggests that LLZ reacts with water at high temperature, decomposes and transforms into other materials.

**Table S1** Composition ratio of the LLZ

	Li	H(estimated)	La	Zr	Nb
Composition	6.4	0	3	1.4	0.6
Prepared LLZ	6.33	0.07	3	1.38	0.59
LLZ-H	5.40	1.0	3	1.38	0.59
LLZ-H + Li <sup>+</sup> provider	6.27	0.13	3	1.38	0.59

The Li/La/Zr/Nb composition in the samples was evaluated using inductively coupled plasma spectroscopy (ICP). The Li/La/Zr/Nb composition ratio for the prepared LLZ particles was evaluated as 6.33/3/1.38/0.59, where this ratio was normalized based on a La stoichiometry of 3.

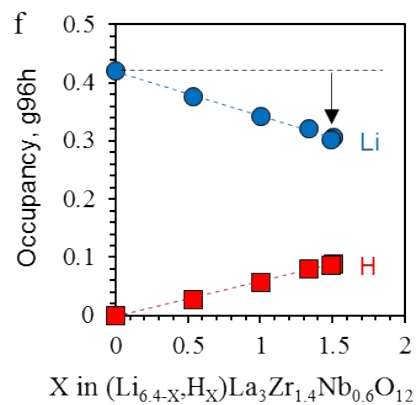
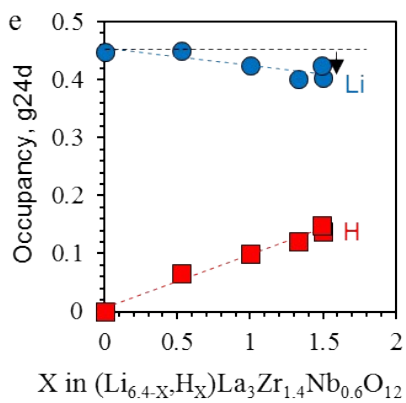
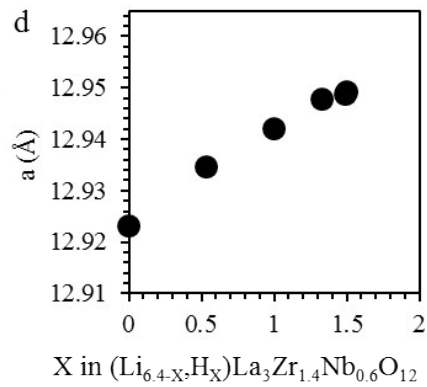
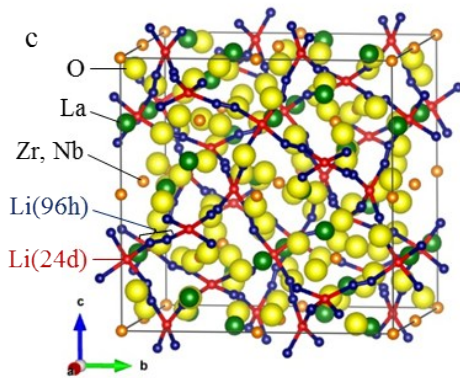
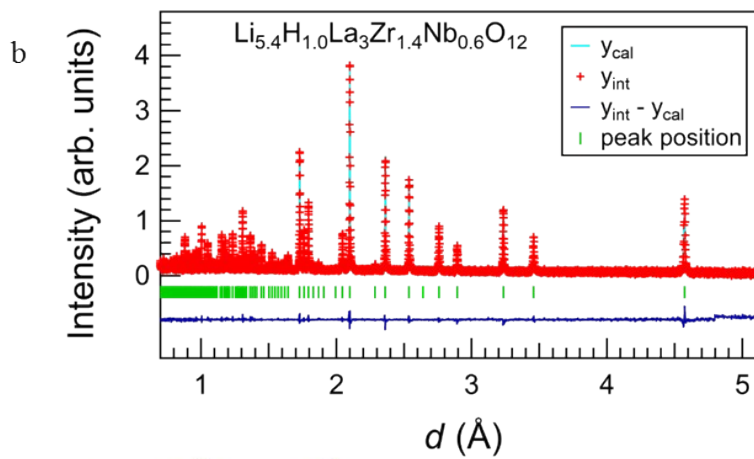
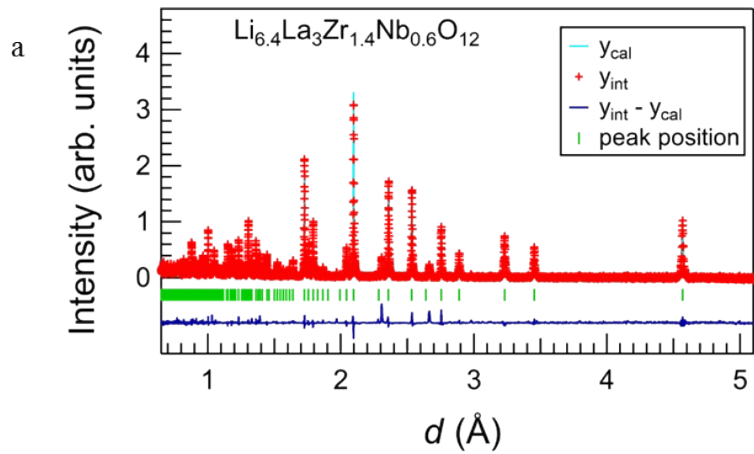


**Figure S2** Neutron diffraction pattern and Rietveld analysis result of (a)  $\text{Li}_{6.4}\text{La}_3(\text{Zr}_{1.6}\text{Nb}_{0.4})\text{O}_{12}$  and (b)  $(\text{Li}_{5.4}\text{H}_{1.0})\text{La}_3(\text{Zr}_{1.4}\text{Nb}_{0.6})\text{O}_{12}$ , respectively. c: Schematic image of the garnet crystal structure.  $\text{H}^+$ -substituted content dependence of the lattice parameter (d), and relative  $\text{Li}^+$  occupancy in tetragonal sites (24d) (e) and octahedral sites (96h) (f).

The sites occupied by  $\text{H}^+$  in LLZ were subsequently investigated using neutron diffraction data and Rietveld refinement. Neutron diffraction data were collected with time-of-flight diffractometers (iMATERIA at the Material and Life Science Experimental Facility of the Japan Proton Accelerator Research Complex). A powder sample was sealed in a 6 mm diameter vanadium cell with an indium ring. The crystal structure for each sample was refined using the Z-Rietveld refinement program [Z-Rietveld] (**Fig. S2a,b**). All crystal structure images were drawn by VESTA [VESTA] (**Fig. S2c**). The crystal parameters for the cubic  $\text{Li}_5\text{La}_3\text{Ta}_2\text{O}_{12}$  garnet structure (Ia-3d) were used as a fitting template for characterization of the garnet phase, as described by Cussen. The lattice parameter was found to monotonically increase with increasing  $\text{H}^+$  substitution from 1.2923(1) nm ( $\text{Li}_{6.4}\text{La}_3\text{Zr}_{1.4}\text{Nb}_{0.6}\text{O}_{12}$ ) to 1.2949(2) nm ( $\text{Li}_{4.9}\text{H}_{1.5}\text{La}_3\text{Zr}_{1.4}\text{Nb}_{0.6}\text{O}_{12}$ ) (**Fig. S2d**). This increase is attributed to the replacement of stronger Li-O bonds by weaker O-H bonds, which suggests that the substituted  $\text{H}^+$

occupies Li sites and diffuses deep into the LLZ particles rather than being located at the surfaces. The dependence of the relative occupancies of H<sup>+</sup> and Li<sup>+</sup> on the substituted H<sup>+</sup> content for both tetragonal sites (24d) and octahedral sites (96h), which are originally Li<sup>+</sup> sites in LLZ, was calculated from Rietveld refinement. The relative Li<sup>+</sup> occupancy in tetragonal sites (24d) remained almost constant with H<sup>+</sup> substitution (**Fig. S2e**), but the Li<sup>+</sup> occupancy in octahedral sites (96h) decreased with increasing H<sup>+</sup> substitution (**Fig. S2f**), which indicates that the Li<sup>+</sup> in octahedral sites (96h) is selectively exchanged with H<sup>+</sup> (Figure S2c), but the H<sup>+</sup> substituted by ion exchange partially occupies both tetragonal sites (24d) and octahedral sites (96h).

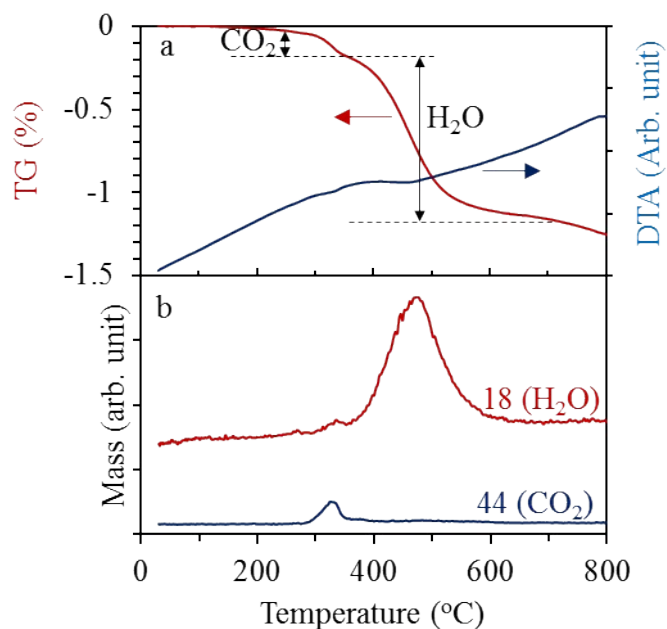


**Figure S3** Thermogravimetric-differential thermal analysis and mass spectrometry of LLZ-H.

The temperature of H<sup>+</sup> release from LLZ particles was confirmed by thermogravimetric-differential thermal analysis (TG-DTA) and mass spectrometry. Two weight loss steps were observed in the TG curve and were identified by mass spectrometry as the release of CO<sub>2</sub> (molecular number: 44) at approximately 300 °C and the release of H<sub>2</sub>O (molecular number: 18) at approximately 400 °C. The temperature for the release of CO<sub>2</sub> from LLZ is 300 °C, which is much lower than the Li<sub>2</sub>CO<sub>3</sub> decomposition temperature, which suggests that only adsorbed CO<sub>2</sub> was present on the LLZ particle

surfaces and that no  $\text{Li}_2\text{CO}_3$  had formed via reaction with the lithium in LLZ. The calculated amount of adsorbed  $\text{CO}_2$  was approximately 0.1%. When H is released from LLZ at 400 °C, the cation and anion charge balance is lost, and LLZ decomposes.

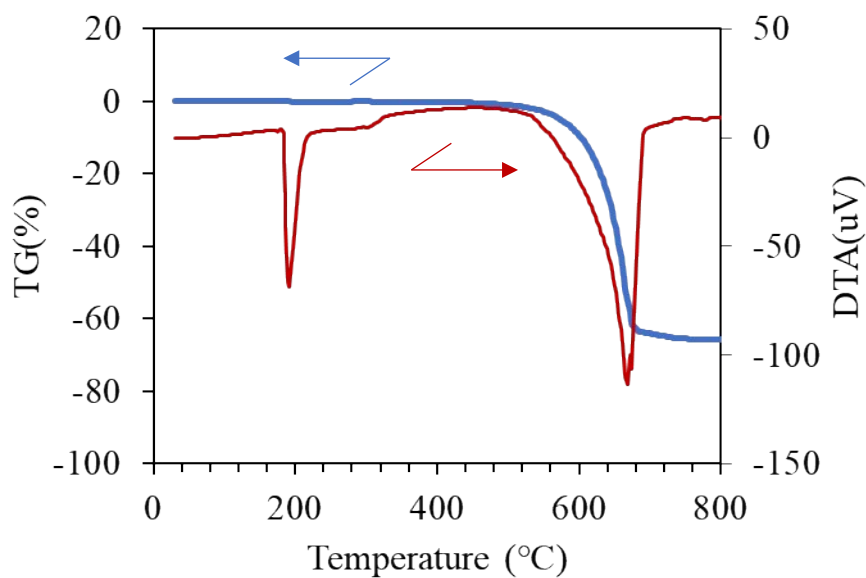


**Figure S4** Thermogravimetric-differential thermal analysis of a mixture of LiOH and LiNO<sub>3</sub>

The melting point of a mixture of LiOH and LiNO<sub>3</sub> was confirmed by thermogravimetric-differential thermal analysis (TG-DTA). Two endothermic reactions at 191°C and 668 °C were confirmed by DTA curves. No weight changes observed at 191 °C, which indicates a melt of this mixture. On the other hand, a drastic weight loss was observed at 668 ° C due to the release of NO<sub>2</sub>.

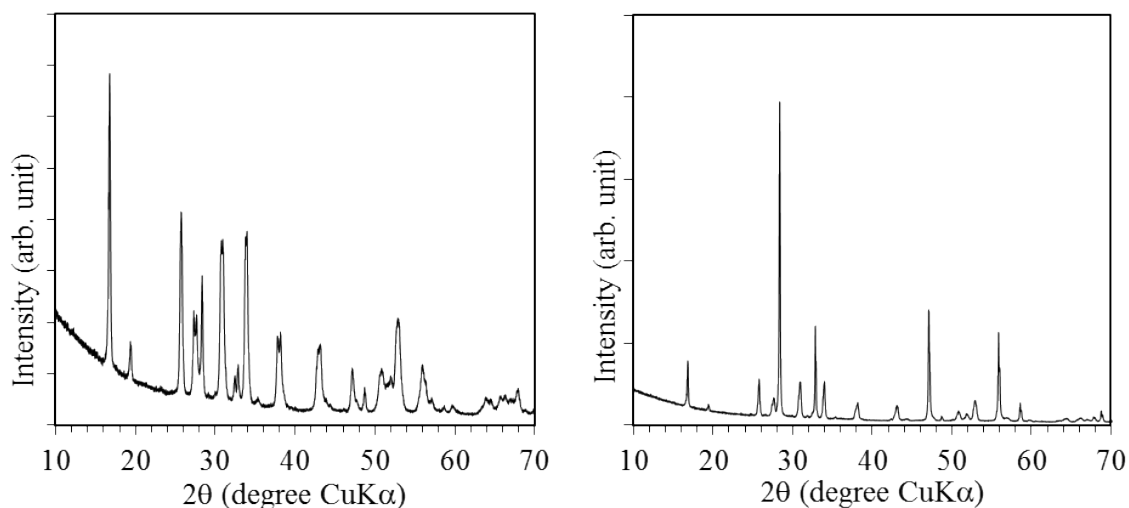


**Figure S5** XRD patterns of a mixture of LLZ-H and LiOH (a) and a mixture of LLZ-H and LiNO<sub>3</sub> (b) after heating at 400 °C.

Only LiOH and LiNO<sub>3</sub> are expected to be potential lithium provider candidates for LLZ, but LiOH was determined to be unsuitable as described in the following. A mixture of LLZ-H and LiOH (mixing ratio: 1:1) was heated at 400 °C; however, the sharp XRD peak for the single-phase cubic garnet structure of LLZ-H was split into peaks of the tetragonal garnet-related phase (space group I41/acd), which were refined by Awaka into the La<sub>2</sub>Zr<sub>2</sub>O<sub>7</sub> composition (JCPDS 080-6524) as the decomposition of LLZ proceeded (Figure S5a). This result suggests that maintaining the cubic-type garnet-type structure is difficult due to the loss of the charge balance, which is likely the result of earlier removal of H<sup>+</sup> from LLZ-H rather than the supply of Li<sup>+</sup> from LiOH because the

melting point of LiOH (approximately 462 °C) is higher than the temperature of the release of H<sup>+</sup> from LLZ-H (approximately 400 °C). Thus, the melting point of the lithium provider should be lower than the temperature of the release of H<sup>+</sup> from LLZ-H (approximately 400 °C).

LLZ-H was then mixed with LiNO<sub>3</sub>, which is the other lithium provider candidate (mixing ratio: 1:1), and this mixture was then heated at 400 °C to evaluate the chemical reactivity. The major XRD peaks were assigned to La<sub>2</sub>Zr<sub>2</sub>O<sub>7</sub> (JCPDS 080-6524), and no diffraction peaks due to LLZ were observed, which indicates decomposition of LLZ-H via chemical reaction with LiNO<sub>3</sub> (Figure S5b). Furthermore, the metal parts in the furnace were conspicuously corroded after heating the mixture, which suggests production of HNO<sub>3</sub> and indicates that the H<sup>+</sup>/Li<sup>+</sup> ion exchange between LLZ-H and LiNO<sub>3</sub> did proceed steadily. However, LLZ was attacked and decomposed via further chemical reaction with the generated HNO<sub>3</sub> because LLZ was easily decomposed by the acid. Thus, LLZ must be protected from the acid atmosphere after the H<sup>+</sup>/Li<sup>+</sup> ion exchange between LLZ-H and the lithium provider. In this study, it was effective to mix equimolar amounts (1:1 ratio) of strong basic LiOH with LiNO<sub>3</sub> to neutralize the strongly acidic HNO<sub>3</sub> generated by H<sup>+</sup> / Li<sup>+</sup> ion exchange between LLZ-H and LiNO<sub>3</sub>. As supporting evidence, the corrosion of metal parts in the furnace was almost

suppressed, indicating that the neutralization reaction has progressed. In preliminary experiments, the ratio of  $\text{LiNO}_3$ :  $\text{LiOH} = 0.75$ :  $0.25$  could not suppress LLZ decomposition. This suggests that the neutralization reaction was incomplete. The ratio of  $\text{LiNO}_3$  and  $\text{LiOH}$  was selected to be 1: 1 from these results.

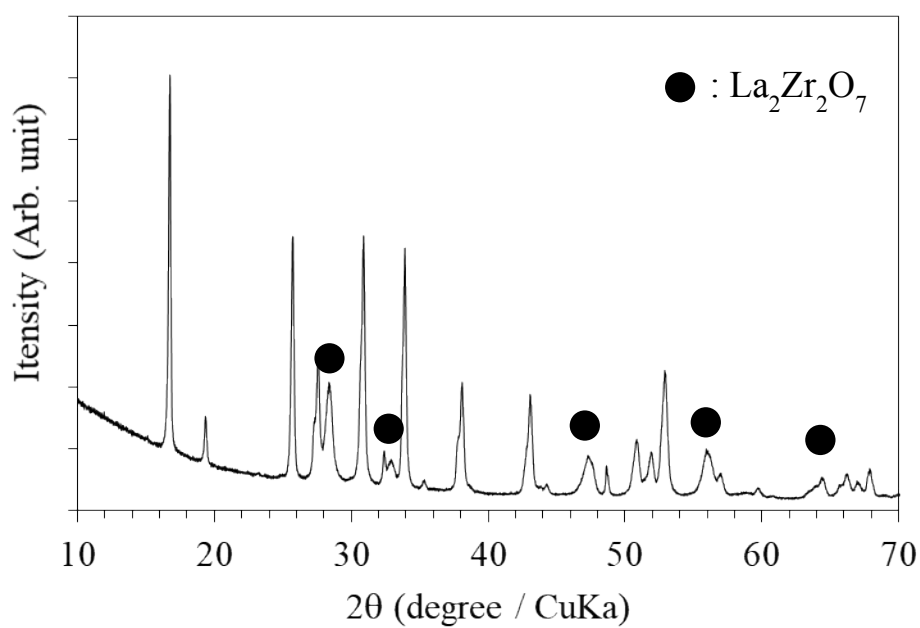


**Figure S6** XRD patterns of only LLZ-H after 600 °C annealing.

LLZ-H could not maintain the charge balance due to the release of  $\text{H}_2\text{O}$  by above 400 °C annealing, which resulted in phase partially change to  $\text{La}_2\text{Zr}_2\text{O}_7$  (JCPDS 080-6524).

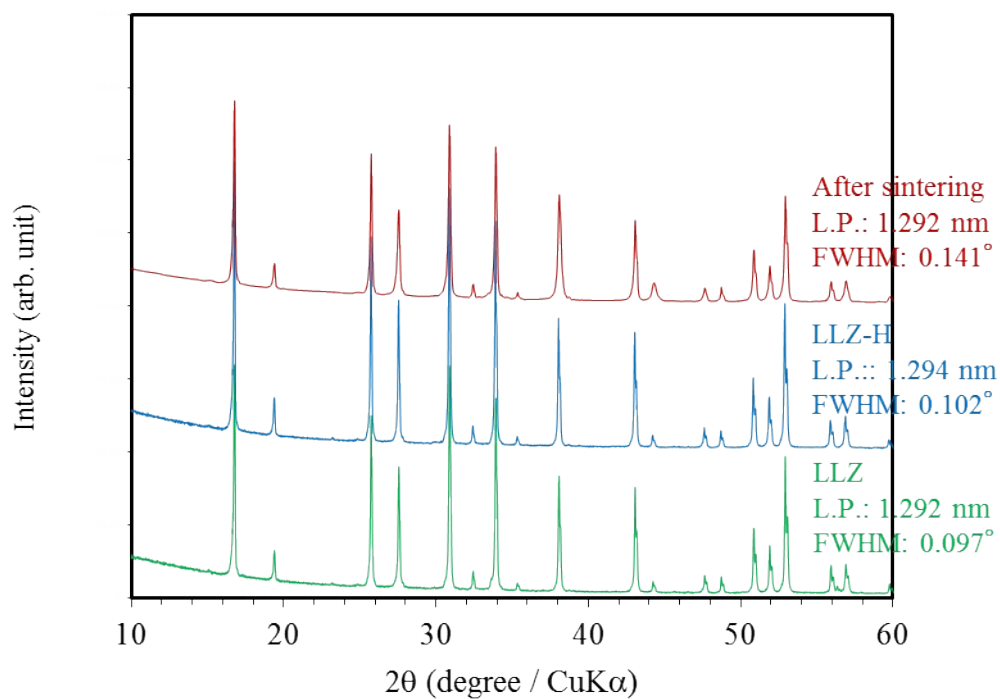


**Figure S7** XRD patterns for LLZ during each treatment.

Particles prepared for this study (bottom),  $\text{H}^+$ -substituted LLZ (LLZ-H) obtained by immersion in water (middle), and a mixture of LLZ-H with  $\text{LiOH}$  and  $\text{LiNO}_3$  after annealing at  $400^\circ\text{C}$  (top).

**Table S2** Relatively densities and conductivities as function of the temperature and pressure

	Relatively density (%)	Conductivity (S cm <sup>-1</sup> @25 C)
300 °C - 98 MPa	< 60	< 10 <sup>-6</sup>
350 °C - 98 Mpa	< 60	< 10 <sup>-6</sup>
400 °C - 0 MPa	65	8.0 x 10 <sup>-6</sup>
400 °C - 49 MPa	69	1.4 x 10 <sup>-5</sup>
400 °C - 74 MPa	78	1.0 x 10 <sup>-4</sup>
400 °C - 98 MPa	90	2.2 x 10 <sup>-4</sup>
400 °C - 196 MPa	89	1.8 x 10 <sup>-4</sup>

Theoretical density: 5.1 g cm<sup>-3</sup>, Typical green density: ~55 %

Below 400 °C sintering, both relatively densities (D) and conductivities ( $\sigma$ ) were still low. This is due to the fact that the H<sup>+</sup> / Li<sup>+</sup> ion exchange reaction did not occur, and sintering did not proceed. Both D and  $\sigma$  drastically increased with increasing the pressure from 0 MPa up to 98 MPa at 400 °C sintering but they did not show any significant pressure dependence above 98 MPa.

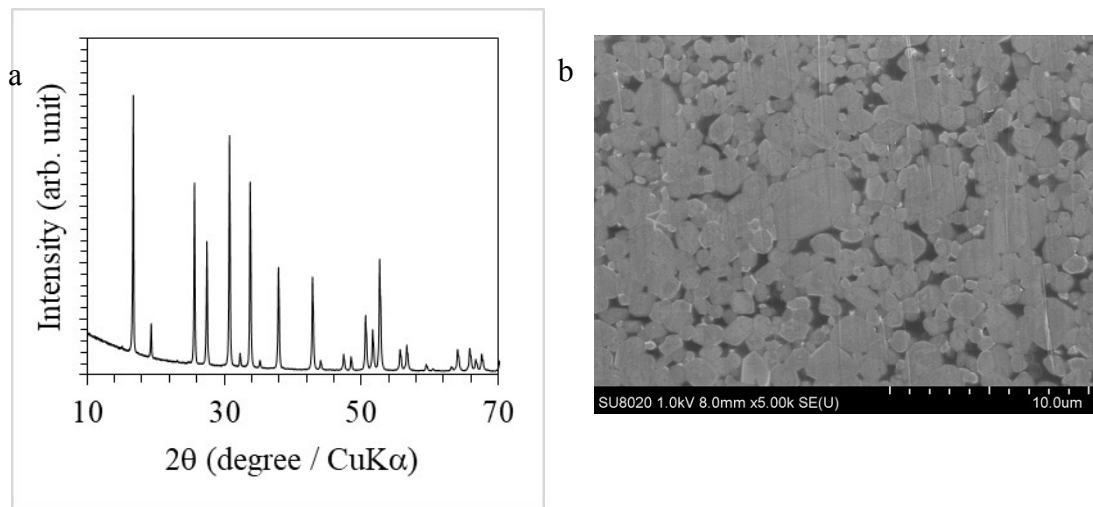
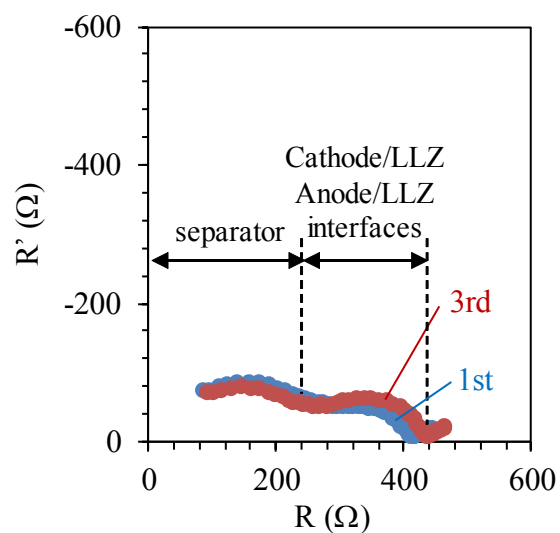
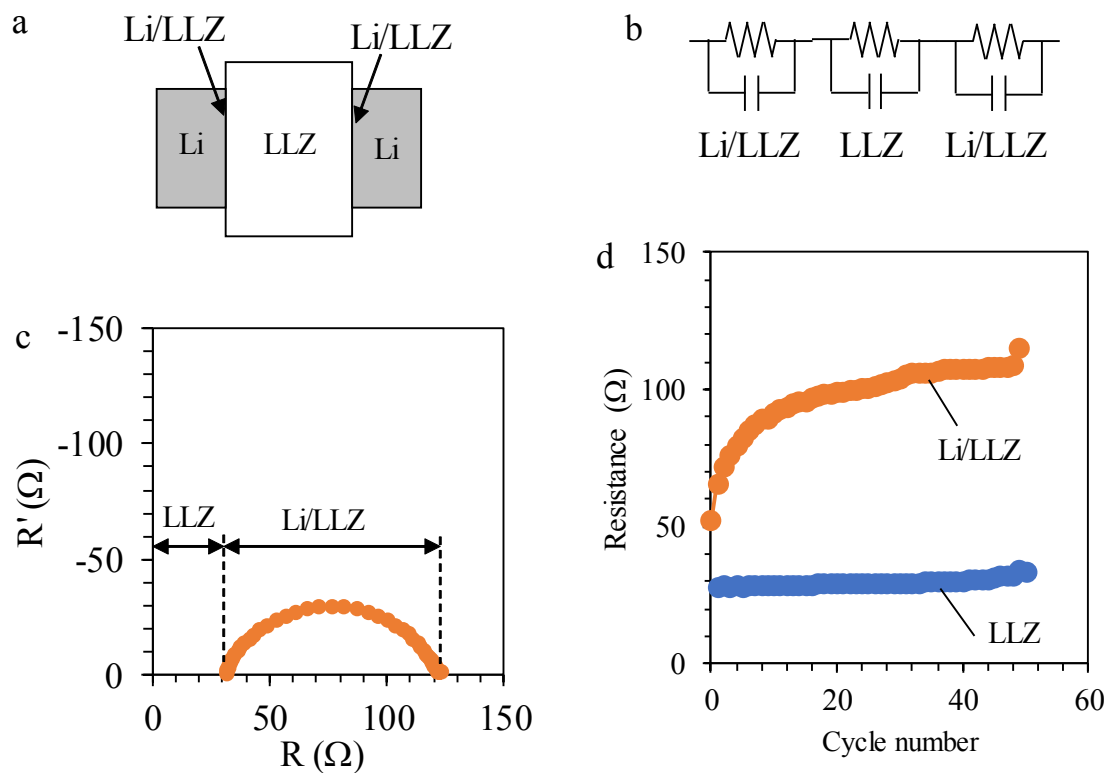


Figure S8 shows the XRD pattern (a) and SEM image (b) of the LLZ polycrystal sample synthesized by conventional thermal sintering (800 °C, 40 h). XRD result confirmed the single phase of a cubic garnet type structure. The relative density and grain size of the sample were  $\sim 90\%$  and  $\sim 3\ \mu\text{m}$ , respectively.



**Figure S9** Nyquist plot of Li/LLZ/NCM+LLZ batteries measured at 4.3 V

The interfacial resistance of the battery was evaluated using a two-probe AC impedance method. Measurements were conducted after charging at 4.3 V vs. Li/Li<sup>+</sup>. The resistance after 3<sup>rd</sup> charging (red circle) is almost the same value with that of after 1<sup>st</sup> charging (blue circle). This indicates that chemical condition at the interfaces was almost stable during 3 cycling.



**Figure S10** A schematic image (a) and an equivalent circuit model (b) of Li/LLZ/Li symmetric cell. Nyquist plot of this Li/LLZ/Li symmetric cell (c). Lithium plating/stripping cycles dependence of LLZ separator and Li/LLZ interfacial resistances (d).

The Li/LLZ/Li symmetric cell was prepared to evaluate the Li/LLZ interface condition during lithium plating/stripping reaction cycles under non-pressure condition (Fig. S10 a). LLZ bulk pellet was prepared at  $\sim 400$   $^{\circ}\text{C}$  and lithium metal was deposited on the LLZ pellet surface by vacuum deposition. The resistance of this cell was evaluated by

AC impedance analysis and the resistance of LLZ separator and Li/LLZ interface can be calculated using an equivalent circuit model (Fig. S10b). The LLZ separator resistance was observed as an X-intercept and the Li/LLZ interfacial resistance was observed as a semi-circle in the Nyquist plot in Fig. S10c. Figure S10d shows the lithium plating/stripping cycles (current density:  $0.5 \text{ mA cm}^{-2}$ , electrical capacity:  $1 \text{ mAh cm}^{-2}$ , temperature:  $60 \text{ }^\circ\text{C}$ ) dependence of LLZ separator and Li/LLZ interfacial resistances. Although, LLZ separator resistance was constant during the plating/stripping cycles, the Li/LLZ interface resistance was gradually increased with increasing the plating/stripping cycles, which indicates that the Li/LLZ condition was changed.